The Southern Oscillation in Surface Circulation and Climate over the Tropical Atlantic, Eastern Pacific, and Indian Oceans as Captured by Cluster Analysis

KLAUS WOLTER

Department of Meteorology, University of Wisconsin, Madison, WI, 53706

(Manuscript received 30 June 1986, in final form 14 November 1986)

ABSTRACT

Clusters of sea level pressure (SLP), surface wind, cloudiness, and sea surface temperature (SST) in the domain of the tropical Atlantic, eastern Pacific, and Indian Oceans are introduced and discussed in terms of general circulation and climate. They appear to capture well the large-scale degrees of freedom of the seasonal fields. In the Atlantic and, to a lesser extent, in the eastern Pacific, most analyzed fields group into zonally oriented "trade wind" clusters. These are separated distinctly by the near-equatorial trough axis. By contrast, the Indian Ocean features strong interhemispheric connections associated with the monsoon systems of boreal summer and, to a lesser degree, of boreal winter.

The usefulness of clusters thus established is elucidated with respect to the Southern Oscillation (SO). General circulation changes associated with this planetary pressure seesaw are deduced from correlation maps of surface field clusters for January/February and July/August. During the positive SO phase (i.e., anomalously high pressure over the eastern Pacific and anomalously low pressure over Indonesia), both the Atlantic and eastern Pacific near-equatorial troughs are inferred to be shifted towards the north from July/August SLP, wind, and cloudiness fields. While eastern Pacific trade winds are weakened in both seasons in the positive SO phase, the Atlantic trades appear strengthened at the same time in the winter hemisphere only. Over the Indian Ocean, the monsoon circulation seems to be strengthened during the positive SO phase, with the summer monsoon displaying a more complex picture. Its SLP, cloudiness, and SST fields support an enhanced southwest monsoon, while its surface winds appear largely inconclusive. SST is lowered during the positive SO phase in all three tropical oceans.

Since all major tropical circulation components over the Atlantic, eastern Pacific, and Indian Ocean participate in the Southern Oscillation, as is evidenced by field significance tests, they become prime movers for the widespread tropical interannual climate variations associated with this global pressure seesaw.

1. Introduction

The interannual variability of the tropical ocean–atmosphere system has recently grown into an intensive research area for meteorologists and oceanographers alike. The Southern Oscillation, in particular, has been the focus of many investigations. Early empirical studies (e.g., Walker and Bliss, 1932) defined this phenomenon as a surface pressure seesaw between the tropical eastern Pacific and Indian Ocean, associated with global rainfall anomalies. Troup (1965) revived the topic by proposing a physical mechanism through which the Southern Oscillation operates, namely a direct thermal circulation cell between the warm Eastern Hemisphere over the Indian Ocean and the cool Western Hemisphere over the Pacific Ocean, later named "Walker cell" by Bjerknes (1969).

Since then, most empirical investigations have focused on the behavior of the Southern Oscillation at the surface of the Pacific Ocean (Reiter, 1979; Egger et al., 1981; Rasmusson and Carpenter, 1982; Newell et al., 1982; Pazan and Meyers, 1982). Other analyses have been directed towards the western dipole of the Southern Oscillation, the Indian Ocean basin (Pant and Parthasarathy, 1981; Nicholls, 1984; Cadet, 1985; Wu and Hastenrath, 1986). Studies concerning the global and, in particular, the extratropical aspects are of lesser interest here (e.g., Hastenrath and Wu, 1982; Pan and Oort, 1983; Wright, 1985).

This paper attempts to analyze in synopsis the large-scale participation of surface fields over the tropical Atlantic, eastern Pacific, and Indian Oceans in the Southern Oscillation. A particular statistical technique—cluster analysis—will be employed to filter lesser scale features. This method was chosen because a straightforward correlation analysis of ship data fields with respect to the Southern Oscillation is hampered by the scarcity of observations in large portions of the tropics (Fig. 1); however, seasonal means of geophysical variables are highly spatially correlated. For instance, Livezey and Chen (1983) show that the monthly mean extratropical Northern Hemispheric 700 mb geopotential height field (resolved into 840 squares) effectively only consists of about 50 spatial degrees of freedom. Barnett and Preisendorfer's (1978) relatively few "key regions" of Northern Hemispheric climatic change are understood in the same fashion. In this context, it appears desirable to delineate which areas behave coher-

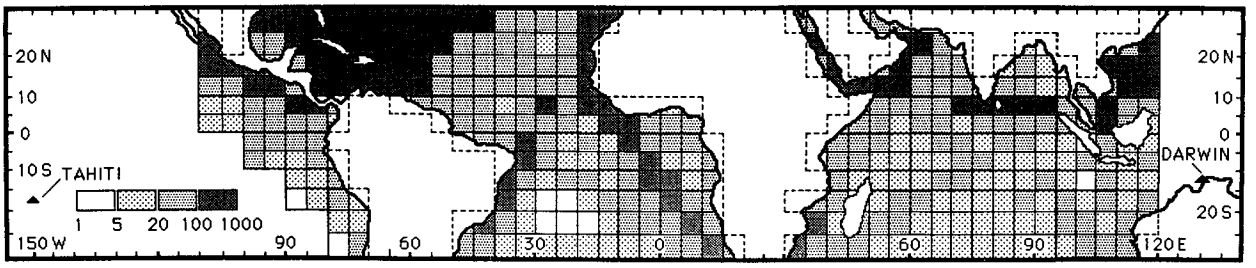

FIG. 1. Orientation map showing density of ship observations by 5° square areas. Numbers indicate calendar monthly averages [total number of observations during the 36 year period 1948–83 divided by 432 = (36)(12)]. Solid triangles mark the locations of the Southern Oscillation index stations Darwin and Tahiti.

ently enough to represent one spatial degree of freedom.

Cluster analysis is shown here to accomplish this objective to a large extent. In fact, its basic purpose is to discover and delineate natural groupings (clusters) of variables (Hartigan, 1975, p. 6; Johnson and Wichern, 1982, p. 534). So far, though, only a handful of cluster analyses may be found in meteorological publications (Gadgil and Iyengar, 1980; Lawson et al., 1981; Galliani and Filippini, 1985). It is conjectured that this is due to arbitrariness in previous cluster size definitions and to the lack of assessments of their statistical significance. Remedies for both drawbacks are proposed here.

It was decided not to apply factor analysis techniques directly on the ship dataset, since the small ratio of temporal versus spatial degrees of freedom in this dataset poses a serious problem to the statistical estimation of the principal components of the field (Storch and Hannoschöck, 1985). In addition, noisiness of the data due to insufficient density of observations would render the explained variance even of the top orthogonal factors small. Large-scale clusters, once established, can be factor analyzed more successfully. Such a companion study has been undertaken, and is being prepared for publication.

Sections 4 and 5 of this paper develop cluster analyses of large-scale surface fields. Practical solutions for the aforementioned problems are proposed in section 4. Detailed results in the form of major clusters of coherent interannual climate variability are presented in section 5 and discussed against background climatology (section 3).

In section 6, characteristics of the Southern Oscillation are examined, as they reveal themselves in cluster fields of sea level pressure, wind speed, cloudiness, and sea surface temperature in the tropical Atlantic, eastern Pacific, and Indian Oceans, correlated with an index of the Southern Oscillation (Parker, 1983). For the first time, such cluster fields are studied in context and compared for boreal winter (January/February) and summer (July/August) from a general circulation perspective. Their field significance is determined with Monte Carlo techniques which will also help to assess the number of large-scale degrees of freedom left in the cluster fields (Livezey and Chen, 1983).

2. Data

Ship observations of sea level pressure (SLP), surface wind, total cloudiness, and sea surface temperature (SST), have been obtained from the National Climatic Center at Asheville, North Carolina, for the tropical Atlantic, eastern Pacific, and Indian Oceans. Their climatic mean fields are presented in detail in atlases by Hastenrath and Lamb (1977, 1979). A condensed version of this data source is utilized here, with monthly means averaged over 391 latitude-longitude squares each (Fig. 1). The geographic locations of Parker's (1983) Southern Oscillation dipoles Tahiti and Darwin are indicated as well in Fig. 1. The 36-year base period 1948–83 is chosen for the following analysis, since it comprises the longest continuous time interval with adequate ship data coverage.

It was decided to focus on the extreme seasons. The bimonthly means of January/February and July/August appear to capture quite well the annual extreme positions and strengths of both the Indian Ocean monsoon systems, as well as the Atlantic and Pacific subtropical high pressure centers and the enclosed near-equatorial trough (Hastenrath and Lamb, 1977, 1979). The majority of 5° squares feature at least 40 observations per season (Fig. 1), while large portions of the Southern hemispheric oceans barely reach 10 observations per season.

If a single month of a season was missing for a 5° square, its value was interpolated in time by averaging the departures from the mean of the preceding and the following months. High month-to-month persistence and the average annual cycle of tropical climate elements is utilized by this interpolation scheme. Spatial interpolation is avoided in order not to distort the subsequent cluster analysis. If both months of a season were missing, the seasonal mean was inserted as a substitute. This lowers absolute correlations with other 5° squares. Thus, 5° squares with frequently missing data cluster at relatively low similarity values (section 5a).

3. Background climatology

In boreal winter (January/February, Fig. 2), the SLP field features a near-equatorial trough sandwiched between subtropical high pressure zones to the north and south (Fig. 2a). The Atlantic and eastern Pacific portions of this trough are rather sharply defined and centered a few degrees north of the equator. Over the Indian Ocean it is much broader and centered south of the equator, with its most conspicuous regional centers around Madagascar and Indonesia. Along with this pressure distribution, northeast trades dominate north of the near-equatorial trough and southeast trades south of it (Fig. 2b).

Clear to partly cloudy skies characterize subtropical high pressure belts, while the near-equatorial trough has embedded in it a zone of convergence and abundant cloudiness, the intertropical convergence zone (ITCZ), defined most sharply over the eastern Pacific, and broadest over the Indian Ocean (Fig. 2c). In addition, the oceanic upwelling regions of the Southern Hemisphere (Fig. 2c, d) tend to be covered with extensive decks of low cloudiness (Hastenrath and Lamb, 1977, p. xi).

A broad band of warm surface waters about the equator characterizes the large-scale tropical SST distribution (Fig. 2d). It is flanked by increasingly cooler surface waters to the north and south, in particular in the eastern portions of the tropical South Pacific and Atlantic where cool eastern boundary currents reign. Conversely, the western portions of the north and south Equatorial Currents transport warm water from the equatorial warm water belt towards the Caribbean and southern South America in the Atlantic, and towards southern Africa in the Indian Ocean. The latter ocean exhibits a cool western boundary current along the Somali coast driven by the northeast monsoon.

In boreal summer (July/August, Fig. 3), all mean surface circulation elements in the Atlantic and eastern Pacific domain are shifted northward compared to the January/February setting. Strengthened cross-equatorial flow is associated with intense oceanic equatorial upwelling and mostly clear skies along the equator (Fig. 3b, c, d). The oceanic upwelling system off northwest Africa shrinks in extent and strength, while the upwelling regions off South America and southwest Africa reach their seasonal peaks with concomitantly extended cloud decks (Fig. 3c, d). Large areas of high SST in the Gulf of Mexico and the neighboring Pacific add to the band of warm surface waters near the equator (Fig. 3d), as compared to the boreal winter (Fig. 2d).

Over the northern Indian Ocean, the summer monsoon entails more drastic changes. Low pressure over south Asia replaces the winter monsoon high pressure (Fig. 3a versus 2a) and results in broad southwesterly flow, with surface wind maxima over the Arabian Sea, the Bay of Bengal, and the South China Sea (Fig. 3b). High SST of the Persian Gulf and the Red Sea are separated from the broad zone of warm surface waters to the east by intense upwelling which takes place off Somalia and Saudi Arabia (Fig. 3d) in response to the strong winds along the respective coast lines (Fig. 3b). While clear wintertime skies near India and Indo-China give way to heavy monsoonal cloud covers, less cloudy skies appear around Indonesia and Madagascar (Fig. 3c). Otherwise, the South Indian Ocean region undergoes little change.

4. Methodology

a. General discussion of cluster analysis

We want to ascertain which geographical areas behave coherently enough in, say, the SST field, to be grouped together as one large-scale degree of freedom. This objective is akin to the central clustering objective of grouping similar objects together (Anderberg, 1973, p. xi; Hartigan, 1975, p. 1). No a priori assumption about the number of groups has to be made (Johnson and Wichern, 1982, p. 532). We do assume, however, that interannual climate variability does not occur randomly in space. In other words, most regions are expected to group with the same neighboring regions for the majority of interannual climate variations. Otherwise few clear-cut clusters would emerge.

The total number of possible ways of sorting n objects into k groups is a Stirling number of the second kind, a prohibitively huge quantity to search through for most practical purposes (Johnson and Wichern, 1982, p. 533). Hence, one needs an algorithm to optimize the sorting. In particular, the clustering of statistical variables (e.g., time series for different squares) is amenable to *joining hierarchical clustering algorithms.* The number of possible groupings is greatly reduced in this method by keeping variables that have entered a cluster inside it for the rest of the analysis (Anderberg, 1973, p. 132; Johnson and Wichern, 1982, p. 543).

Once a quantitative measure of similarity between clusters is defined, it can be used to optimize the search for groups. With regard to statistical variables and their departures from respective means, the correlation between two of them best reflects quantitatively how similar they are (Anderberg, 1973, p. 75). A positive correlation of $+1.0$ would represent the most similar coupling, compared to -1.0 for the least similar possible pairing.

At the beginning of the cluster analysis, each statistical variable is a cluster in itself, in fact the very simplest kind possible. Proceeding from such single variable clusters to more complex ones, the following *joining hierarchical clustering algorithm* for N variables is widely used (after Johnson and Wichern, 1982, pp. 543–544):

1) Search the correlation matrix of all clusters for the most similar pair of clusters (highest correlation).

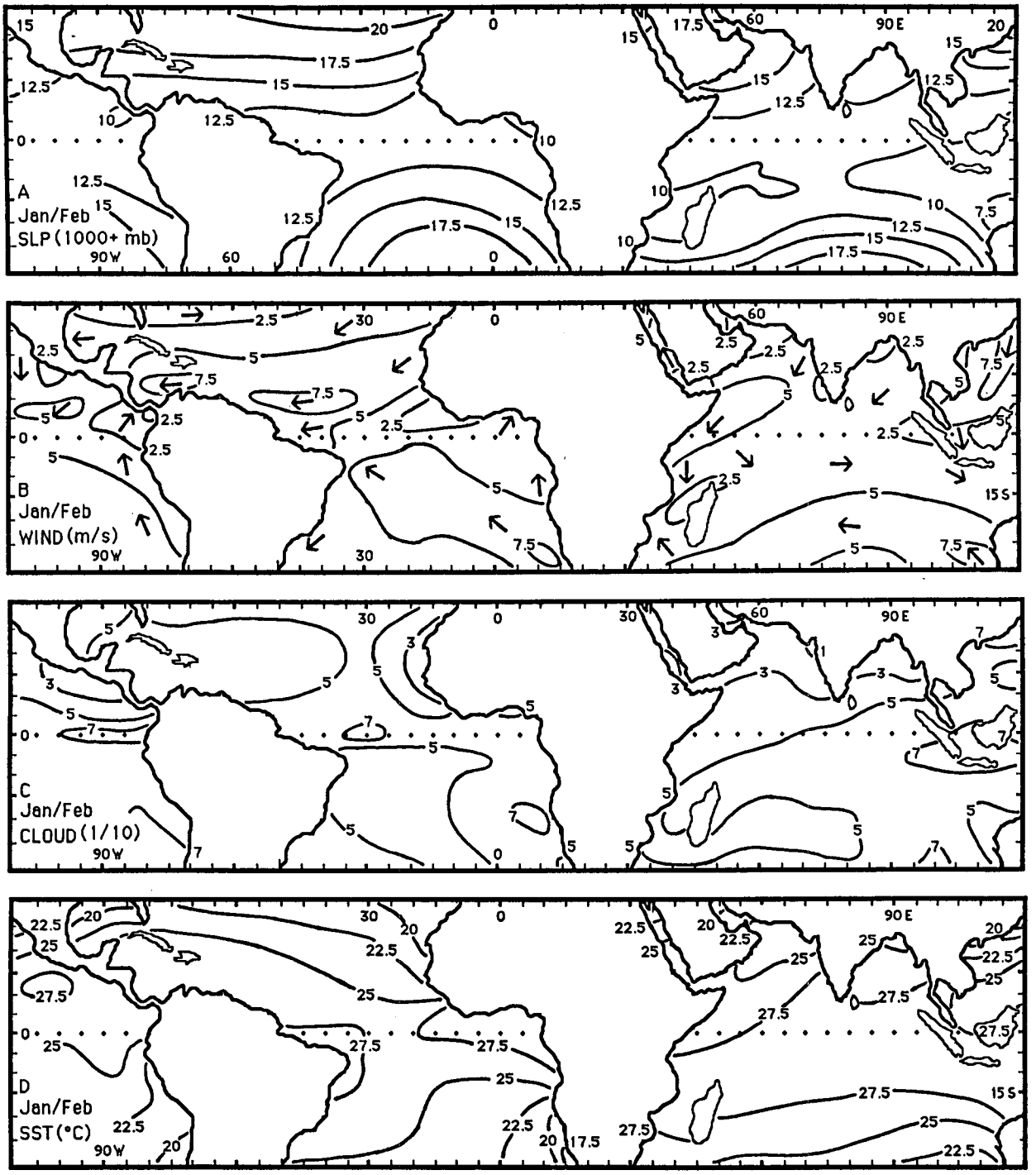

FIG. 2. January/February mean fields (1948–83) of a) sea-level pressure, in (1000+)mb, b) wind speed, in m s^{-1}, and selected directional wind arrows, c) total cloudiness, in tenths, and d) sea surface temperature, in °C.

Let this correlation between most similar clusters x and y be r_{xy}.

2) Merge clusters x and y. Label the newly formed cluster, e.g., (u). Update the entries in the correlation matrix by (a) deleting the rows and columns corresponding to clusters x and y and (b) adding a row and a column giving the similarities ("correlations") between cluster (u) and the remaining clusters.

3) Repeat steps 1 and 2 a total of $N - 1$ times. (All objects will be in a single cluster at termination of the

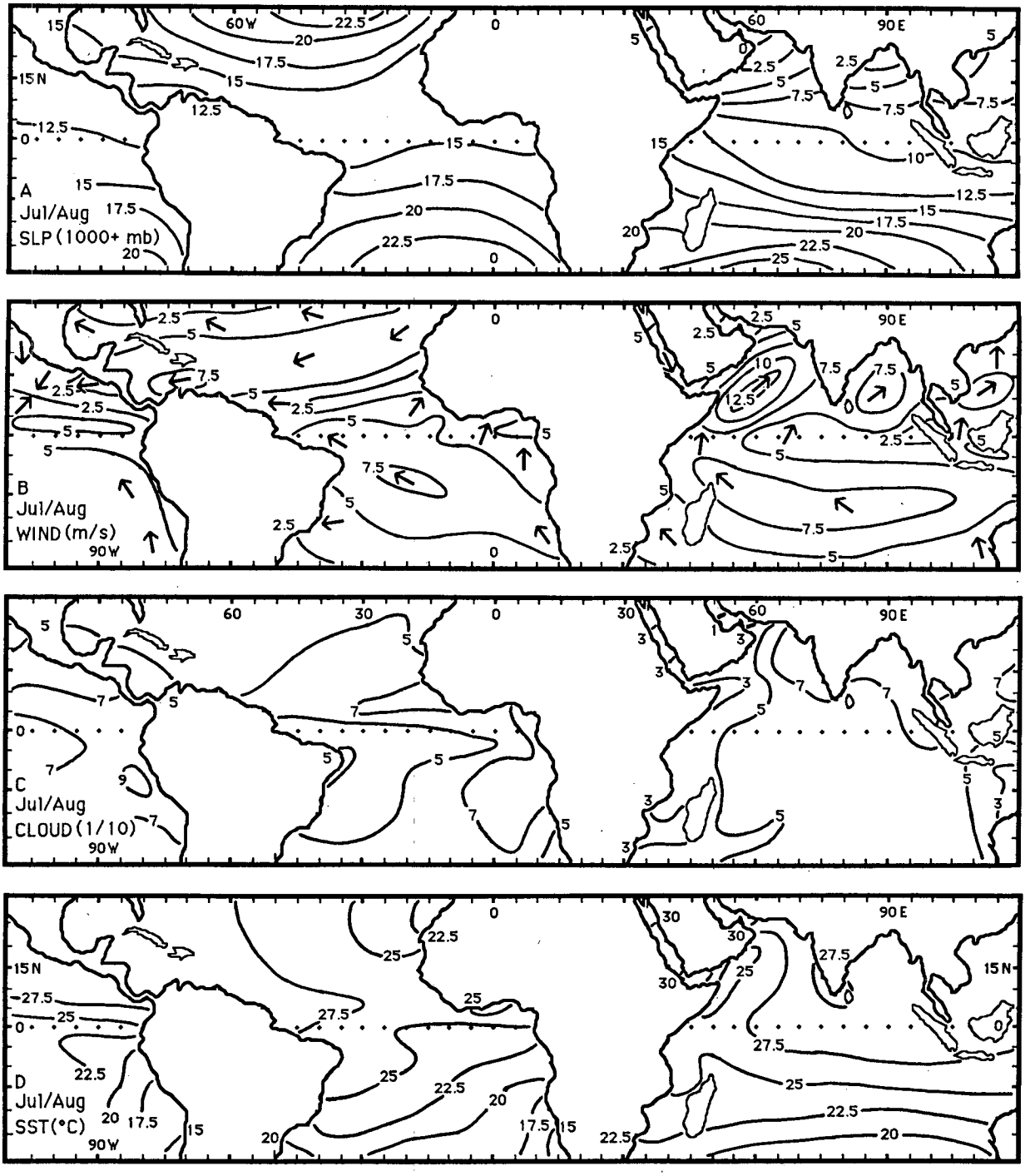

FIG. 3. As in Fig. 2, except for July/August mean fields.

algorithm.) Record the identity of clusters that are merged and the similarities at which the mergers take place.

The crucial step (2b) of assigning similarities ("correlations") among clusters of more than one statistical variable each is often taken in one of three possible different ways. One can either use the maximum correlation of single variables between cluster (u) and, e.g., cluster (v), called *single linkage method, or* the minimum correlation between variables belonging to (u) and (v) (*complete linkage method*), *or* the average cor-

relation between all variables in (u) on the one side and all variables in (v) on the other (*average linkage method*).

In the context of this study, single linkage clusters appear particularly vulnerable to noisy time series which may be grouped into a cluster by accidental correlation with just a single time series inside the cluster. With growing cluster size, quite dissimilar time series can accumulate in such a cluster, a process called "chaining" (Anderberg, 1973, p. 138; Johnson and Wichern, 1982, p. 548). Towards the other extreme, complete linkage clusters accept a new member only if all present members correlate well with it. This keeps such clusters small and hard to relate to each other (Anderberg, 1973, p. 173).

The average linkage method is chosen as the most suitable one for the present purposes. It appears less vulnerable to slight errors ("noise") in the similarity measure, and less prone to "chaining" (Hartigan, 1975, p. 209 and p. 200, respectively). All three clustering methods yield roughly the same cluster configurations for strong similarity structures (Johnson and Wichern, 1982, p. 554).

For more than two statistical variables, the *average similarity* (or *correlation*) $r_{(uv)}$ between clusters (u) and (v) is determined by:

$$r_{(uv)} = \sum_{i=1}^{N_u} \sum_{j=1}^{N_v} r_{x(i)y(j)}/(N_u N_v) \qquad (1)$$

where $r_{x(i)y(j)}$ is the correlation coefficient between variable $x(i)$ in cluster (u) and variable $y(j)$ in cluster (v), and N_u and N_v are the number of variables in clusters (u) and (v) (Johnson and Wichern, 1982, pp. 552–553).

Tree diagrams are one possible way of illustrating the information computed with (1). In Fig. 4, a highly simplified example of a correlation matrix and an associated tree diagram is given. Variables 1, 2 as well as 4, 5 are merged first, since they have the highest similarities. The final cluster (1–6) features the average similarity 0.60, merging (1–3) and (4–6). Since these smaller cluster were merged earlier, at higher similarities, 0.60 constitutes a *minimum* estimate of the mean correlation $m_{1\text{-}6}$ among all variables:

$$m_{1\text{-}6} = (1/15) \sum_{i=1}^{5} \sum_{j>i} r_{ij}. \qquad (2)$$

The value $m_{1\text{-}6} = 0.68$ is indeed higher than the average similarity of (1–6).

b. *Employed clustering procedure*

Two major obstacles have to be removed on the road to clustering 391 time series in any of eight different meteorological element–seasons. For one, we have to decide whether it is more sensible to cluster the complete dataset at once, or whether to split it into subsets. Secondly, we want to select among all clusters those intermediate ones that come closest to capturing the spatial degrees of freedom of the field.

The first problem can be approached from two different viewpoints. For statistical significance reasons, it is advisable to have a high ratio of cases to variables, especially if small correlations prevail. However, we expect strong correlations to permeate the field. With too small a data subset, one would encounter many clusters straddling or exceeding the examined subdomain boundaries. This was verified with boreal winter SST in the Atlantic. The extent and location of many of its clusters depended on the number of cluster variables admitted, as long as this number stayed below about 50. Conversely, analyzing the whole dataset at once would increase the chances for spurious teleconnections. It would be more expensive as well, in particular with respect to subsequent Monte Carlo tests. On balance, the data base was kept separated in its natural geographic domains: the three oceanic basins of tropical Pacific, Atlantic, and Indian Ocean. Certainly SST, but also SLP, wind speed, and cloudiness fields tend to separate quite clearly into these domains, at least in the long-term average fields (Hastenrath and Lamb, 1977, 1979).

Turning towards the crucial question of how to differentiate among all analyzed clusters, the hierarchical

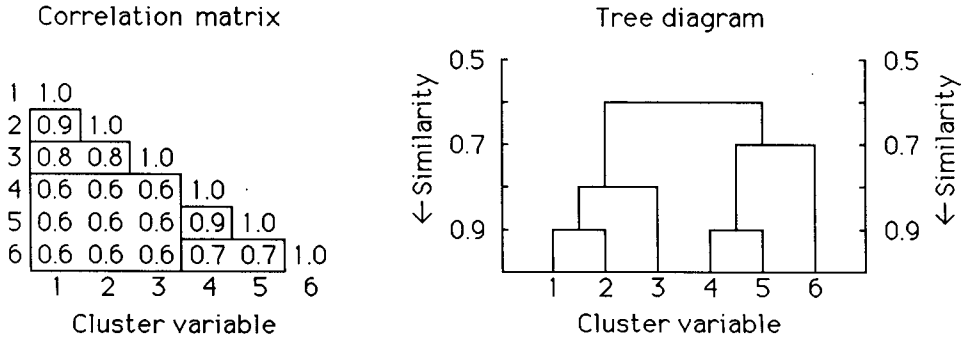

FIG. 4. Simplified correlation matrix and tree diagram scheme of six clustered variables.

structure of building clusters from small units to larger, more complex ones suggests the following organizing principle: let a cluster remain on its level of complexity as long as only clusters of *lower* levels merge into it.

Single variable clusters and the final all-encompassing cluster aside, four complexity levels, in ascending order named δ-, γ-, β-, and α-level, were required for an effective differentiation scheme in our oceanwide clustering studies:

1) δ-level: only single variables are concatenated, combining 2 to rarely 5 variables.
2) γ-level: two or more δ-clusters have been merged; as long as only δ-clusters or single variables are joined with present γ-cluster, it stays at this level of complexity with 4 to about 12 variables.
3) β-level: two or more γ-clusters have been merged; as long as lower level clusters or single variables are joined with present β-cluster, it keeps its level, ranging from 8 to sometimes over 40 variables.
4) α-level: two or more β-clusters have been joined; as long as lower level clusters or single variables are joined with existing α-cluster, it keeps its level and a range up to the final cluster (45 for the Pacific, 167 for the Atlantic, and 179 for the Indian Ocean).

With some oceanwide α-clusters on one side, and impractically small γ- and δ-clusters on the other (less likely to survive the testing procedure described in section 4c), large-scale circulation features are apparently best captured by β-level clusters, averaging around 20° by 20° latitude–longitude.

c. *Statistical significance testing of individual clusters*

After having analyzed oceanwide datasets into clusters, it appears desirable to determine their statistical significance. As no specific analytic procedure was at hand for this purpose, Monte Carlo simulations were used. This technique has gained popularity among meteorologists with its usefulness for a variety of statistical significance problems in geophysical applications (Barnett and Preisendorfer, 1978; Livezey and Chen, 1983).

Employing Quenouille's (1952, p. 168) procedure, it was found that year-to-year persistence of tropical seasonal averages can reduce the temporal degrees of freedom by up to 20%. Hence, 30 cases instead of 36 were used in the Monte Carlo simulations. The Atlantic, eastern Pacific, and Indian Ocean datasets were emulated by 180, 45, and 180 random variables with normal distributions, respectively. Twenty Monte Carlo cluster analysis runs each were performed with such random variables. For lower size clusters, these provided hundreds of similarities to construct empirical estimates of the appropriate 95% significance levels. For larger clusters, similar estimates are still considered reliable since 95% levels barely differed from 90% levels.

Whenever a β-cluster similarity surpassed the appropriate 95% Gaussian noise clustering similarity, it was kept unchanged for further use. If not, it was dismantled step by step into smaller original cluster parts of the β-, γ- or even δ-level, continuously checking for significance. As soon as all cluster parts of the biggest, yet significant size were determined, the search was stopped and these significant cluster parts replaced the old cluster in the subsequent analysis. If no significant lower level cluster parts were found, the original cluster was completely withdrawn from further consideration. Finally, if a single five degree square did not cluster with its immediate neighbors, but with some remote area, it failed a continuity screening test and was dropped from the analysis.

d. *Computation and field significance testing of Southern Oscillation correlation fields*

This section supplies the background for the computations analyzed in section 6. It describes the construction of area-weighted cluster time series, the statistical determination of local and field significance, and the inference onto the degrees of freedom present in the cluster field.

For the construction of cluster time series, the area a_k of each original 5° square was weighted according to the areal proportion of its sea surface times the latitudinally dependent size of the full 5° square. In all, eight element–seasons i, normalized departure time series X_{ikl} for all years l of the record were calculated. This type of time series was chosen, since the correlation matrix (and not for instance the covariance matrix) was originally used to determine the clusters.

Hence, normalized, area-weighted time series $C_{j(i)l}$ of cluster $j(i)$ in element–season i was constructed according to:

$$C_{j(i)l} = \forall\Big(\sum_{k \ni j(i)} a_k X_{ikl}\Big) / \forall\Big(\sum_{k \ni j(i)} a_k\Big). \tag{3}$$

Up to 50% missing data for any given cluster and season were ignored in the employment of (3). If more than 50% of the data were missing in (3), a rare event, seasonal averages were substituted for the missing data, analogous to the procedure described in section 2.

For the computation of local significance levels, the SOI used was found to have negligible year-to-year persistence. Hence, the conventional double-sided t-test for correlation coefficients could be applied, with N-2 = 34 everywhere. A correlation coefficient of $|r| = 0.329$ served, thus, as the cutoff threshold for the 95% significance level with the Southern Oscillation index.

The finite number of clusters and their potential interdependence requires the testing of *field significance* as well as *local significance* in SO correlation fields, a goal commonly pursued using Monte Carlo techniques (Livezey and Chen, 1983). To this end, the SOI was randomly scrambled 1000 times. The scrambling was achieved by 1) drawing for each run 36 uniformly dis-

tributed random numbers, 2) sorting these numbers in ascending order (along with a yearly index for the SOI) and 3) reshuffling the SOI values according to the "sorted" yearly index. After each shuffle, the scrambled SOI values were newly correlated with the unchanged cluster time series fields. The number of correlation coefficients exceeding the 95% *local significance value* of $|r| = 0.329$ were counted, stored, and tabulated at the end of 1000 runs in order to determine the 95% *field significance* threshold. Since no changes in the statistical distributions of either SOI or cluster time series were undertaken, a measure of field significance was thus obtained, however crudely. Possible changes of the SOI's autocorrelation structure are ignored.

Finally, the percentage of clusters needed to reach 95% field significance can be plotted as a function of the number of clusters in the field. Using the binomial distribution, one can graph the percentage of statistically independent 95% significance tests that are passed 5% of the time by chance, as a function of the performed number of tests (Livezey and Chen, 1983). On comparison, if the cluster values fell close to the independent values, the true degrees of spatial freedom would be essentially captured by the cluster field, at least with respect to the Southern Oscillation. If the true number of degrees of freedom were found to be substantially less than the number of clusters indicated, the clusters would have failed to achieve their purpose at least with respect to the Southern Oscillation (section 6).

5. Cluster analysis results

a. General discussion

The average linkage method described in section 4 was used to cluster all three ocean datasets; 167, 45, and 179 5° squares in each of eight element–seasons were entered in the analysis for the Atlantic, Pacific, and Indian Ocean, respectively. They were handled by an appropriate statistical software package (BMDP, 1983). Average correlations of all clusters (i.e., prior to significance testing or level assignments) are summarized in Fig. 5. Thresholds for 95% significance similarities are included.

Large clusters between, say, 10 and 100 5° squares stand a better chance of surviving the Monte Carlo screening than small clusters (Fig. 5). This result suggests a higher regional stability of planetary-scale circulation features, compared to lesser-scale circulation systems, over the tropical oceans. From here on, a cluster is called "strong" ("weak") if it clearly (barely) exceeds the 95% noise threshold.

While the Atlantic tends to have stronger clusters at large scales (10 to 50 5° squares), the Indian Ocean

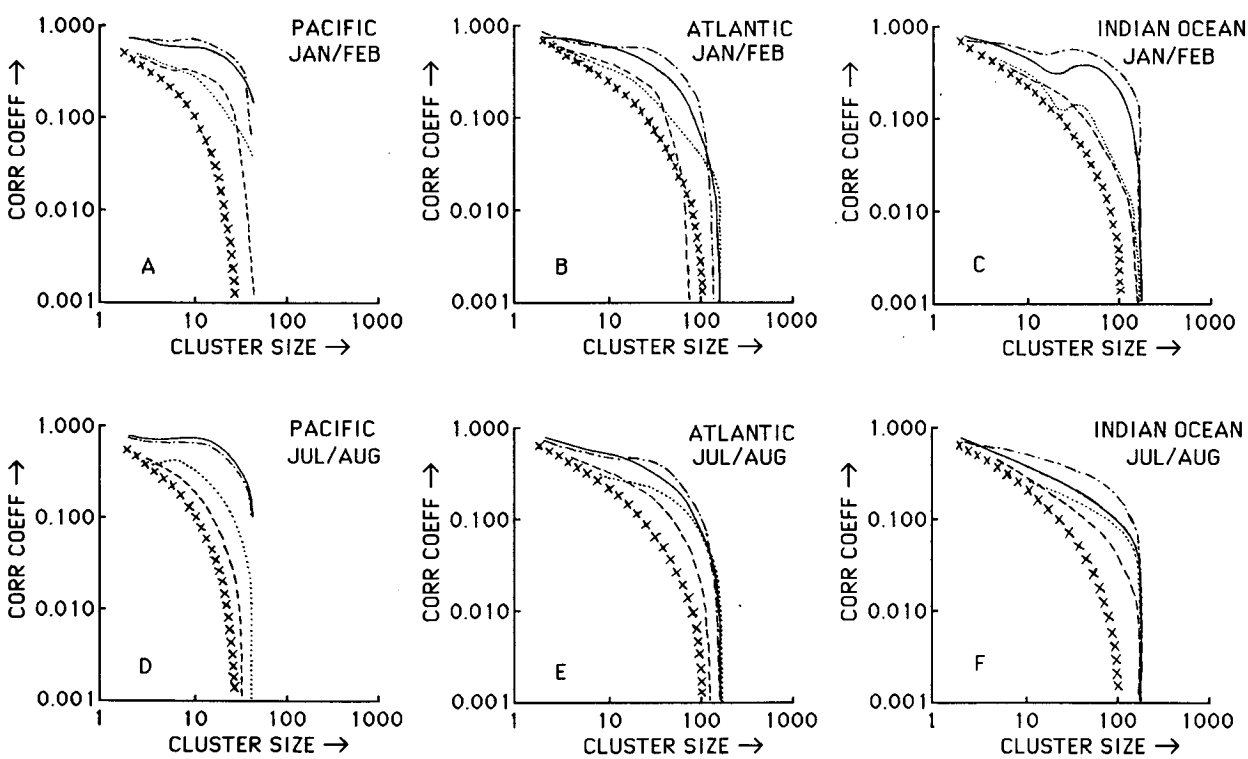

FIG. 5. Average clustering similarities ("CORR COEFF") of sea surface temperature (solid line), sea-level pressure (dash-dotted line), wind speed (broken line), and cloudiness (dotted line) for January/February and July/August, respectively, in the (a and d) eastern Pacific, (b and e) Atlantic, and (c and f) Indian Ocean. The 95% clustering similarities of Gaussian noise (crosses) are added for reference.

prevails on very large scales beyond 50 5° squares (Fig. 5). The SLP clusters in general appear strongest among all elements in Fig. 5, in particular for about 20 to 100 5° squares. The inherent observational noisiness of ship-observed SLP (Hastenrath and Lamb, 1977, p. vii) is apparently outweighed by a high degree of large-scale organization in the tropical SLP fields. The SST clusters are similarly strong, especially over smaller scales and in the eastern Pacific (Fig. 5). Although wind speed is the best observed element at sea (Hastenrath and Lamb, 1977, p. vii), its average similarities drop off considerably compared to SLP and SST (Fig. 5). Cloudiness stays closest to the 95% Gaussian noise threshold values, indicating randomness in its seasonal distribution (Fig. 5). Towards very large scales, it catches up with SLP and SST, denoting common ground in the general circulation of the atmosphere.

Application of the Monte Carlo and continuity screening (reference section 4c) removed, on the average, 21% of the original 5° squares (15.5% of the total area) from the analysis. The scarcity of observations (Fig. 1) can be invoked for many of these removals, in particular in the Southern Hemisphere. A much stronger dependency on the analyzed atmosphere–ocean element is evident: SLP and SST fields have only 4 to 10% of their ocean area coverage removed, as compared to 20 to 31% for cloudiness and wind fields (Figs. 6 and 7).

Similarities of SLP, wind, cloudiness, and SST β-clusters are displayed in Table 1. Pacific, Atlantic, and Indian Ocean clusters are prefixed P, A, and I, respectively. They pertain to all clusters and cluster parts left after the Monte Carlo and continuity screening described in section 4c. Whenever the original β-cluster or β-cluster part did not represent one continuous area, but several such areas, it was broken down into these areally connected portions without changing the original similarity or significance. Such cluster portions could be alluded to as teleconnections. They are kept separated for this study, until more can be said about their links. The total number of clusters and cluster portions varies from 26 to 40 (Table 1).

Similarities of clusters depend more on the specific atmosphere–ocean element than on season or region (Table 1). The strength of clusters, as measured in 1/100 excess over 95% significance thresholds, reaches more than +20 for many SLP and SST clusters, but rarely more than +10 for wind and cloud clusters. For comparison, a 99% significance threshold would lower the achieved excess by only about 5. With Southern Hemispheric clusters being about 10/100 weaker than Northern Hemispheric clusters, a link of strength to density of observations (Fig. 1) can be inferred.

b. *Cluster fields*

The spatial distribution of all clusters listed in Table 1 is shown in Fig. 6 for boreal winter (January/February) and in Fig. 7 for boreal summer (July/August). Only selected clusters are discussed here against the background climatology of Figs. 2 and 3.

During boreal winter (January/February, Fig. 6), a large cluster (P1) encompasses the eastern Pacific low pressure trough (Fig. 6a). The near-equatorial trough systems of the Atlantic and Indian Ocean (Fig. 2a) are divided along their axes by members of the same α-cluster, each one to the north and south (Fig. 6a). Some of the stronger clusters (A1, A2, A7, I2, I9, and I10 in Fig. 6a) connect these trough zones with their respective hemispheric subtropical high pressure belts (Fig. 2a).

Reflecting a similar organizing principle, the core regions of the trade wind regimes (Fig. 2b) stand out with clusters A3, A4 in the Northern Hemisphere, and A12, I13 in the Southern Hemisphere (Fig. 6b). Over the eastern Pacific, P1 and P3 are portions of the same β-cluster. Northeast and southeast Pacific trades thus behave sympathetically (as proposed by Reiter, 1979). The most prominent feature in the Indian Ocean wind cluster field is the eastern branch of northeast monsoonal winds over the South China Sea, including its recurving part over Indonesia (I4, Fig. 6b).

Dominant cloudiness clusters (P2, A3, I3, I4; Fig. 6c) are located in the Northern Hemisphere where they bridge relatively clear skies in the subtropics (Fig. 2c) with large cloudiness values at their southern margins. The strong clusters A1 and I7 appear as variations on this theme (Fig. 6c) by connecting as well to enhanced cloudiness in the north. The cloud bands of the Atlantic and Indian Ocean ITCZ cluster poorly, perhaps due to randomness in their structure.

The strong SST cluster P2 (Fig. 6d) encompasses the eastern Pacific equatorial warm water belt and the upwelling area off the west coast of South America, linked by the Peru Current (Pickard and Emery, 1982, p. 186). Equatorial regions of high SST in the Atlantic and Indian Oceans (Fig. 2d) separate along their axes into clusters A7, I5, and I8 to the north, and clusters A8, I9 as well as cluster parts I11 and I13 to the south (Fig. 6d). These axes coincide with equatorial counter currents in both oceans (Pickard and Emery, 1982, pp. 139 and 209). Clusters A8 and I8 appear to capture the cores of the South Equatorial Currents in the Atlantic and Indian Oceans (Fig. 6d). Eastern boundary currents are closely linked to the adjoining North and South Equatorial Currents in Fig. 6d (A4, A9, and much weaker in I10).

In boreal summer (July/August; Fig. 7), the SLP troughs of the Atlantic and eastern Pacific (Fig. 3a) separate along their axes in the cluster field (Fig. 7a). The strongest and largest North Atlantic cluster is located to the west of its winter position (A1 in Fig. 7a and A2 in Fig. 6a), reflecting the mean seasonal westward shift of the Azores high (Hastenrath, 1985, p. 128). Over the Indian Ocean, two major interhemispheric clusters (I4, I11; Fig. 7a) bridge high SLP in the Southern Hemisphere with low SLP over southern

TABLE 1. Similarities of β-clusters in 1/100 (one and two asterisks represent 10/100, and 20/100 excess over the 95% significance level, respectively); clusters with several portions document similarity and significance with the first cluster portion, while the other cluster portions refer to the first one.

Cluster	SLP-I	WIND-I	CLOUD-I	SST-I	SLP-II	WIND-II	CLOUD-II	SST-II
P1	42**	05	09	54**	36**	00	20	65**
P2	70**	29	10	52**	44**	21*	14*	47**
P3	—	(P1)	(P1)	40	44*	(P1)	(P1)	60**
P4	—	—	—	24	—	—	—	53*
A1	45**	34	23*	16	40**	17	40	31**
A2	41**	15	28*	49**	32**	24*	20*	37**
A3	41*	46**	21*	(A1)	36	46	18	25*
A4	34	28**	15	42**	54	(A1)	(A2)	35**
A5	(A4)	68	18	34	30**	13	68	(A3)
A6	37**	19	(A2)	(A5)	(A2)	18	(A3)	12
A7	36**	73*	(A4)	43**	48**	22	20*	(A6)
A8	29	23	(A5)	28**	45**	(A5)	(A7)	26
A9	—	50	(A1)	34**	(A5)	(A5)	21	—
A10	—	(A2)	18	(A1)	(A7)	65	40	—
A11	—	(A6)	(A2)	(A8)	61*	62	—	—
A12	—	23	(A3)	28	71*	(A5)	—	—
A13	—	(A6)	(A4)	—	34	50	—	—
A14	—	(A2)	60	—	58	—	—	—
A15	—	(A2)	—	—	32	—	—	—
I1	33*	10	21	46*	33	15	15*	13
I2	45**	19	18	18	41*	14	14	(I1)
I3	60	14	26*	33*	32**	19*	67	70*
I4	70*	(I3)	29*	25*	34**	(I1)	19	16
I5	(I1)	(I2)	14	45**	(I3)	(I3)	(I1)	21*
I6	33	15	(I2)	34*	20	(I1)	(I2)	72*
I7	59**	(I6)	27*	43**	72*	(I3)	(I1)	(I1)
I8	27	(I2)	33	43**	(I6)	23*	15	20
I9	55**	(I2)	22	(I4)	21*	11	21	33**
I10	40**	17	(I1)	21	33*	(I1)	19	66
I11	38*	13	(I5)	(I7)	(I9)	(I8)	(I8)	(I4)
I12	53*	(I1)	(I8)	59*	—	29	44	(I5)
I13	(I6)	24	62	(I7)	—	(I2)	(I9)	30
I14	27	20	(I7)	(I2)	—	(I3)	(I8)	36*
I15	(I8)	(I2)	(I5)	44**	—	36	(I1)	—
I16	61	(I10)	—	—	—	(I8)	60	—
I17	—	(I3)	—	—	—	(I3)	—	—
I18	—	—	—	—	—	(I9)	—	—
I19	—	—	—	—	—	(I2)	—	—
I20	—	—	—	—	—	(I1)	—	—
I21	—	—	—	—	—	(I9)	—	—
I22	—	—	—	—	—	(I12)	—	—
I23	—	—	—	—	—	65	—	—
I24	—	—	—	—	—	44	—	—

Asia (Fig. 3a). Cluster portions I3, I5 and I6, I8 link monsoonal low pressure systems across India and Indochina, respectively (Fig. 7a).

In the wind speed cluster map (Fig. 7b), the eastern Pacific keeps the interhemispheric connection between cluster portions P1 and P3 shifted northward, compared to Fig. 6b. Over the Atlantic, the strongest and largest cluster is located to the west of its winter position (compare A2 in Fig. 7b against A4 in Fig. 6b), analogous to the pressure cluster field. The core of the South Atlantic trade winds (Fig. 3b) is shifted to the west as well and weakened (A12 in Fig. 7b and A12 in Fig. 6b), possibly due to its reach into data sparse areas (Fig. 1). Wind speed clusters over the Indian Ocean (Fig. 7b) display the most complicated structure of all analyzed fields. The prominent clusters I5 and I8 (Fig. 7b) capture all three mean monsoonal wind speed maxima over the Arabian Sea, the Bay of Bengal, and the South China Sea (Fig. 3b). A close link is inferred between Arabian Sea and Bay of Bengal monsoonal flow (I5).

Strong cloudiness cluster parts (A2 and A4, Fig. 7c) are again noted to be bridging relatively clear skies in the Atlantic subtropics (Fig. 3c) with large cloudiness at their equatorward margins. The Indian Ocean features one strong analogous cloudiness cluster over the Arabian Sea (I1 in Fig. 7c). It links small cloudiness values off Somalia with abundant cloudiness close to

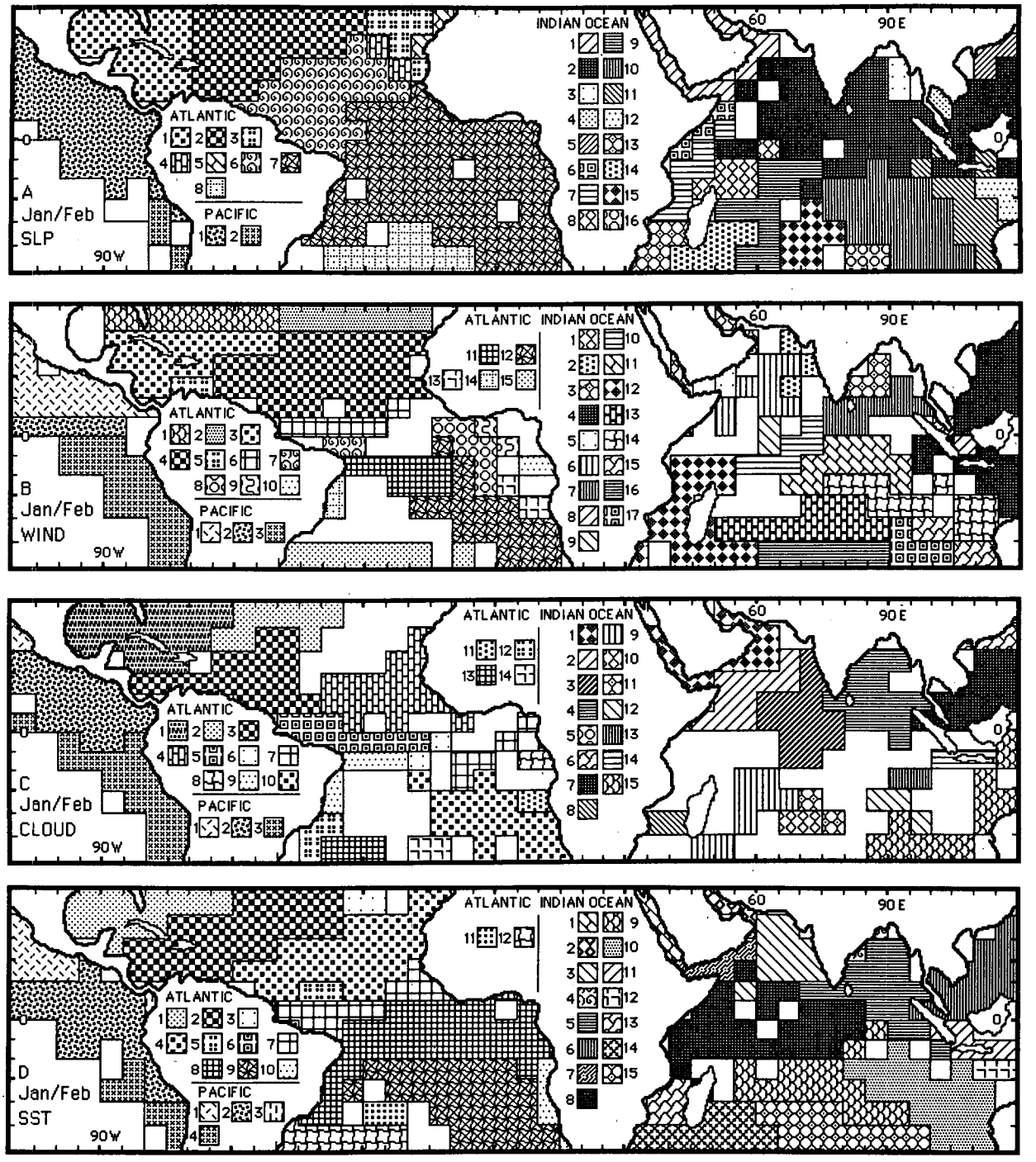

FIG. 6. January/February β-cluster distribution maps (1948–83) of a) sea-level pressure, b) wind speed, c) total cloudiness, and d) sea surface temperature. In each map legend, all patterns are listed with their ocean domain (P Pacific, A Atlantic, and I Indian Ocean) and code number. Similar patterns depict related clusters within each map (i.e., members of the same α- or β-cluster); enhanced patterns represent strong clusters.

India (Fig. 3c), a remarkable testimony of coherent monsoonal behavior over this part of the Indian Ocean.

As in boreal winter, we find the strongest clusters of the season in the SST field of the eastern Pacific (P1, P2; Fig. 7d). The North Atlantic SST is grouped into two strong members of the same α-cluster: A1 encompasses the enlarged (A7 in Fig. 6d) northern portion of the tropical warm surface water belt (Fig. 3d); A2

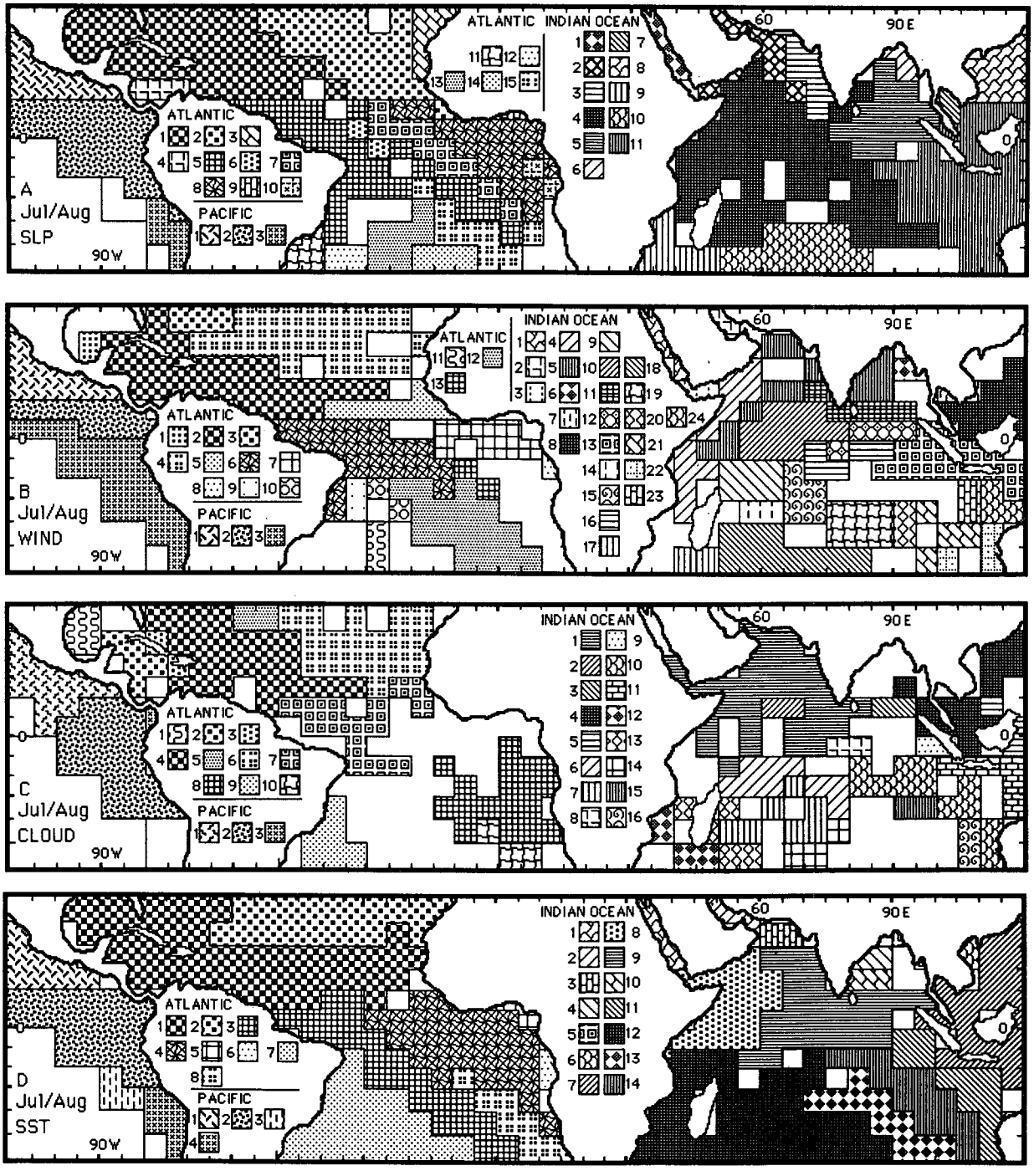

FIG. 7. As in Fig. 6, except for July/August β-cluster distribution maps.

indicates the Canary Current (A4 in Fig. 6d). The South Atlantic eastern boundary current is captured by A4 (Fig. 7d). The western half of the Southern Indian Ocean subtropical gyre (strong I12) and the upwelling region of the Western Arabian Sea (I8) are closely related parts of the same α-cluster, linked by the Somali Current (Pickard and Emery, 1982, p. 209). Similar interhemispheric connections are evident across the South China Sea (I7 in Fig. 7d). The southwest monsoon current (Pickard and Emery, 1982, p. 209) is clustered into strong I9.

In sum, the boreal winter season over the Atlantic and Indian Ocean is characterized by a division of the near-equatorial low pressure trough systems along their

axes (Fig. 6a). Strong clusters connect these trough segments with adjacent subtropical high pressure. The core trade wind regions stand out as strong clusters (Fig. 6b). Relatively clear skies in the subtropics are bridged by major clusters with cloudier skies at their equatorward margins (Fig. 6c). Equatorial bands of high SST are separated roughly along their axes, possibly via equatorial counter currents (Fig. 6d). Eastern boundary currents link closely to the adjoining equatorial currents, reflected in well clustered SST. All four ocean-atmosphere elements achieve highest clustering similarities in conjunction with the trade wind circulation.

The outlined organization principles are repeated for July/August in the Atlantic Ocean domain (Fig. 7), in unison with a northward shift of the main circulation features and a westward shift of their foci. Over the Indian Ocean, strong interhemispheric clusters emphasize the oceanwide character of the summer monsoon system. Throughout both seasons, eastern Pacific SLP and SST clusters strongly relate to the eastern dipole of the Southern Oscillation, while wind clusters show a tendency for northeast and southeast trades to wax and wane synchronously.

6. The Southern Oscillation

a. General results

Of several available indices of this planetary-scale phenomenon (summarized in Wright, 1985), Parker's (1983) Southern Oscillation Index (SOI) is particularly straightforward, based as it is on the sea level pressure difference between the Southern Oscillation dipoles Darwin and Tahiti (Fig. 1). Among stations with long SLP records, these two best represent the Southern Oscillation in coherence and amplitude (Chen, 1982). A positive phase of the Southern Oscillation is defined by anomalously high Tahiti SLP and anomalously low Darwin SLP. Bimonthly averages of this SOI were correlated with all cluster time series, as is documented in Table 2 (displayed in map format in Figs. 8 and 9, section 6b).

Sixty-five of a total of 248 clusters (or 26%) reach the local 95% significance level ($|r| = 0.329$). Many of these correlations are substantially stronger. For instance, ten of them reach the local 99.99% significance level ($|r| = 0.604$). Boreal winter features more distinct relationships than boreal summer. SLP and SST achieve higher correlations than cloudiness and wind, as noted before for (and not independent from) the similarity values reached by the same clusters (Table 1).

At the bottom of Table 2, the first line sums up the percentage of clusters reaching local significance for each field. The second line shows the respective percentage value that was reached by 5% of 1000 Monte Carlo runs with a randomly scrambled SOI being correlated against the very same cluster field (reference section 4d). Six out of eight fields achieve 95% field significance. The bottom line lists the difference between the number of cluster portions (26 to 40) and the number of large-scale degrees of freedom of the field (26 to 48), inferred from a binomial distribution graph (reference section 4d; Livezey and Chen, 1983). Given that these numbers stay small, we feel encouraged in our belief that cluster analysis is capable of compacting seasonally averaged atmosphere–ocean data into their respective large-scale degrees of freedom.

In addition to the correlation analysis, both composite studies and linear regression analyses between SOI and all cluster time series were undertaken. They essentially corroborate all results discussed below in section 6b, in particular inferences on gradients of field where the correlation coefficients are of the same sign.

b. Cluster correlation fields

In January/February (Fig. 8), significant positive correlations with SLP clusters are found over the eastern Pacific and the Caribbean (Fig. 8a). Hence, the domain of the eastern dipole of the SO extends well into the Atlantic. Over the South Atlantic and eastern Indian Ocean, two large areas of significant negative correlation (Fig. 8a) indicate close ties to the western dipole of the SO. Classical descriptions of the SO appear thus corroborated (Walker and Bliss, 1932; Troup, 1965; Berlage, 1966).

Wind speed clusters (Fig. 8b) show for the positive SO phase significantly weakened trades (Fig. 2b) over the eastern Pacific. Bjerknes (1969) had suggested earlier that the trade winds off South America would be weaker during the *negative* phase of the SO, while the North Pacific Hadley circulation (i.e., the northerly surface wind component) would be enhanced. Reiter (1979) corroborated Bjerknes' assertion about the strengthened Hadley cell for the Pacific as a whole. More recently, Egger et al. (1981) and Pazan and Meyers (1982) examined the December–February Pacific wind field for 1947–73, resolved into 2° latitude by 10° longitude bands. Their correlation studies find essentially no dependence of the northeast Pacific trades on the SO, while the southeast Pacific trades appear slightly *strengthened* for a positive SOI over portions of the discussed domain (Fig. 1). Rasmusson and Carpenter (1982) composited six El Niño events from 1951 to 1972, using a finer spatial resolution (2° by 2° latitude–longitude). During the "mature" phase of such an event (December–February), they analyzed strengthened trades to the north and south of the eastern Pacific equator, in corroboration with the present results.

For the North Atlantic and South Indian Ocean, Fig. 8b indicates for the positive SO phase strengthened trades, significant over the North Atlantic. Reiter (1979) reported the Atlantic trades to behave "independently" from the Pacific trades. Pan and Oort (1983) analyzed marginally stronger trades for a pos-

TABLE 2. Correlation coefficients SOI versus β-clusters in 1/100 (one and two asterisks represent 95% and 99% local significance level, respectively). The last three lines list percentage of clusters significant at the local 95% level for each field, required percentage to reach 95% field significance according to Monte Carlo tests, and excess of degrees of freedom in cluster field compared to binomial distribution.

Cluster	SLP-I	WIND-I	CLOUD-I	SST-I	SLP-II	WIND-II	CLOUD-II	SST-II
P1	+56**	−36*	−29	−63**	+33*	−30	+27	−51**
P2	+04	−15	−33	−78**	+75**	+53**	+27	−56**
P3	—	−49**	−05	−40*	+57**	−11	+13	−36*
P4	—	—	—	−26	—	—	—	−47**
A1	+52**	+02	−65**	+10	−26	+16	+15	−02
A2	+27	−16	−37*	−36*	−53**	−33*	+05	−16
A3	+02	+44**	+30	−06	−29	−00	+13	+15
A4	−05	+42*	+10	−22	+43**	+03	−06	+06
A5	−12	−04	+16	−17	−24	+10	−19	+20
A6	−28	−23	−34*	−10	−29	−10	+22	+17
A7	−50**	−35*	+14	−30	−28	−11	+25	−00
A8	−09	−14	−10	−27	−24	+22	+12	−03
A9	—	+04	−47**	−26	+14	+28	−16	—
A10	—	−13	+24	+11	+02	+17	−17	—
A11	—	−29	−08	−35*	+08	+10	—	—
A12	—	+13	+12	−08	+17	+31	—	—
A13	—	−07	+00	—	−04	+02	—	—
A14	—	−13	−28	—	−02	—	—	—
A15	—	+14	—	—	−16	—	—	—
I1	−54**	−01	−18	+02	−38*	−16	+35*	−15
I2	−68**	+25	−16	−10	−46**	−23	+24	−05
I3	−52**	+35*	−17	−39*	−34*	+15	+15	−04
I4	−41*	+40*	+27	−32	−51**	−15	+17	−06
I5	−35*	+05	−06	−62**	−53**	−11	+06	+00
I6	−33*	+01	−23	−45**	+08	+21	−06	+14
I7	−48**	−23	+55**	−50**	−38*	−28	+31	+28
I8	−28	+21	−02	−64**	−13	−30	−08	−33
I9	−32	−10	−21	−54**	−41*	−01	+22	−40*
I10	−56**	−09	−00	−28	−18	−02	+33*	+08
I11	−78**	+06	−05	−73**	−72**	−19	+56**	+11
I12	−43**	+05	+06	−48**	—	+32	−01	−28
I13	−25	+01	−03	−40*	—	−57**	+10	−18
I14	−07	−01	+57**	−10	—	+00	+03	−19
I15	−22	+31	+38*	−12	—	−14	+30	—
I16	−08	−01	—	—	—	−29	−18	—
I17	—	+21	—	—	—	−23	—	—
I18	—	—	—	—	—	−02	—	—
I19	—	—	—	—	—	−29	—	—
I20	—	—	—	—	—	−07	—	—
I21	—	—	—	—	—	+03	—	—
I22	—	—	—	—	—	+32	—	—
I23	—	—	—	—	—	−00	—	—
I24	—	—	—	—	—	−13	—	—
Σ (*; **)	50%	20%	22%	45%	45%	08%	10%	19%
Monte Carlo	15%	12%	12%	14%	13%	12%	13%	14%
Δ (dof)	0	−12	−13	+2	−6	−8	−8	−8

itive SOI over Atlantic and South Indian Ocean, in support of present results. Close to the Indonesia-Australian dipole of the SO, and over the Western Bay of Bengal, the northeast monsoon correlates positively with the SOI (Fig. 8b). A similar result has been described for the extreme western Pacific (Egger et al., 1981; Rasmusson and Carpenter, 1982; Pazan and Meyers, 1982).

Seen in a general circulation perspective, SLP and wind correlation fields (Figs. 8a, b) support each other well. Positive SLP correlations in the region of the eastern Pacific trough (compare Fig. 2a against 8a) translate into raised pressure levels for a positive SOI. Reduced meridional pressure gradients to the north and, in particular, to the south result, entailing weakened trade winds (negative correlations) over the same areas (P1, P3 in Table 2; Fig. 2b against 8b). Conversely, positive SLP correlations over the subtropical North Atlantic and negative SLP correlations over the equatorial Atlantic (Figs. 2a and 8a) imply a steepened meridional pressure gradient during the positive phase of the SO. This corresponds to strengthened North Atlantic trade

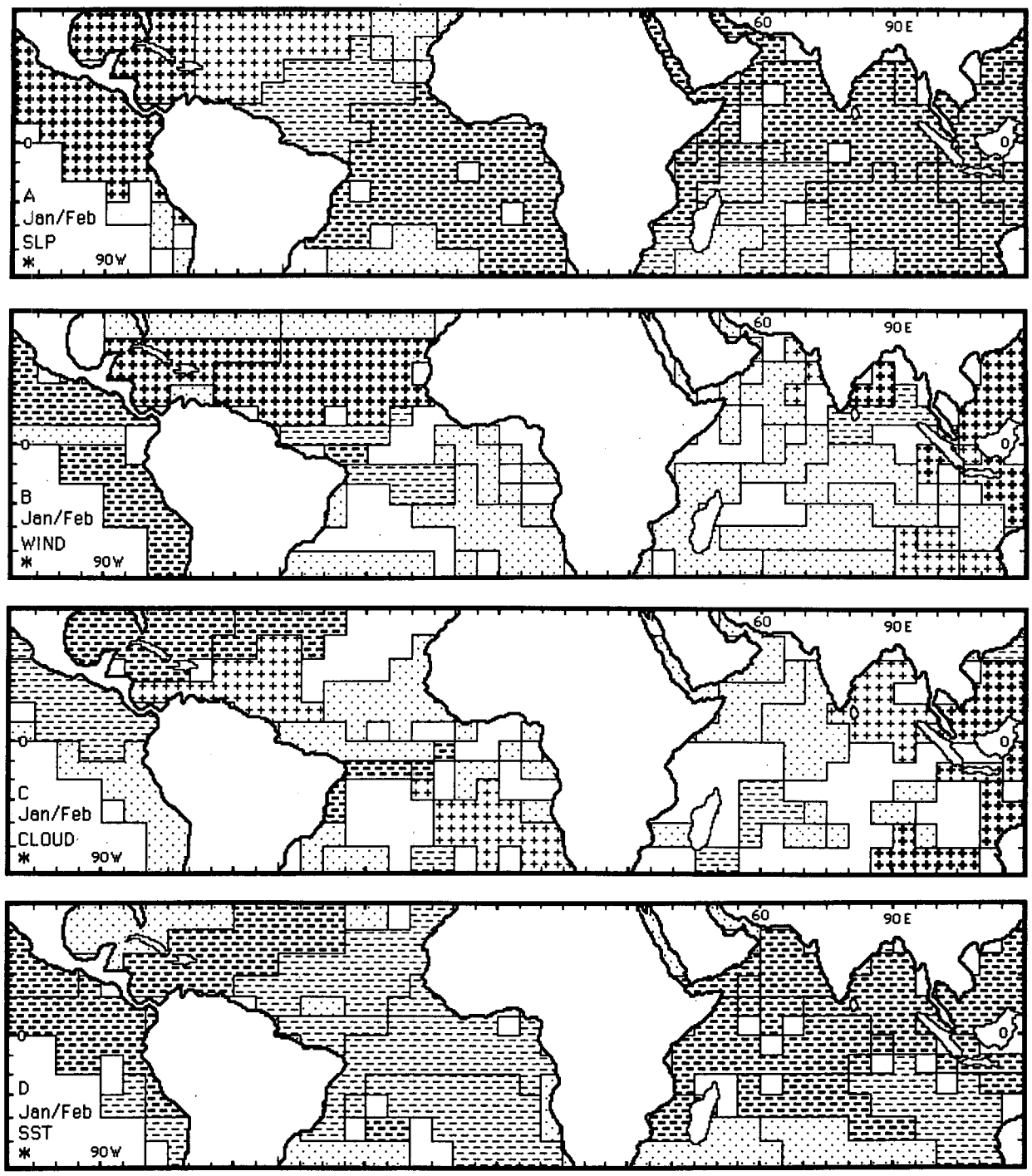

FIG. 8. January/February correlation maps of Southern Oscillation Index (Parker, 1983) vs β-clusters for a) sea-level pressure, b) wind speed, c) total cloudiness, d) sea surface temperature. Enhanced symbols represent 95% local significance levels. Dot raster indicates absolute correlation coefficients not exceeding 0.20. No reduction of temporal degrees of freedom was found (Quenouille, 1952, p. 168), since the used SOI has negligible year-to-year persistence. Fields achieving 95% field significance are marked by an asterisk in the bottom left corner of the map.

winds, as deduced from positive correlations (Fig. 2b and 8b). In conjunction with weakened cross-equatorial flow off Northeast Brazil (negative correlations in Fig. 8b), a southward shift of the Atlantic near-equatorial trough during the positive SO phase is suggested. Over the Indian Ocean, the strongest negative correlations

in the equatorial trough zone (I2, I11 in Table 2; Fig. 2a and 8a) entail steepened meridional pressure gradients to the north and south. Correspondingly, positive correlations in Fig. 8b indicate more vigorous northeasterly monsoonal flow over the Gulf of Bengal and the South China Sea, and enhanced southeast trades over the South Indian Ocean.

Decreased cloudiness during the positive phase of the SO (Fig. 8c) characterizes the eastern Pacific and, in particular, the Caribbean and northwest tropical Atlantic. A similar regional pattern had already been noted by Walker and Bliss (1932) for the seasonal rainfall distribution. The Indian Ocean cloud field correlates significantly positively over the easternmost portion close to the western dipole of the SO (Fig. 8c). For the positive phase of the SO, this translates into anomalously cloudy skies over this area. As indicated by negative correlations in Fig. 8a, during the positive phase of the SO the SLP over the equatorial Indian Ocean is lowered, while positive correlations in Fig. 8b denote anomalously strong northeast monsoonal flow over the South China Sea. The implied wind anomaly pattern appears consistent with enhanced convergence and hence increased cloudiness at the western dipole of the SO.

The circumglobal SST signal (Fig. 8d) during boreal winter is a negative correlation, i.e., an anomalously cold sea surface during the positive phase of the SO, in particular in the eastern Pacific, West Central Atlantic, and the North and equatorial Indian Ocean (Table 2). Such a more or less uniform behavior has been noted previously (e.g., Hastenrath and Wu, 1982). In the North Atlantic, strengthened trade winds during the positive SO phase (Fig. 8b) accompany a relatively cold eastern boundary and equatorial current (Fig. 2d and 8d). The eastern Pacific SST field with its lowered values during the positive phase of the SO (Fig. 8d) complements the SLP signal of concurrently increased sea level pressure at the eastern dipole of the Southern Oscillation (Fig. 8a). In the eastern Indian Ocean, both increased wind stress and cloudiness are associated with anomalously cold SST for a positive SO phase (Fig. 8b, c, d; Hackert and Hastenrath, 1986).

During boreal summer (July/August, Fig. 9), significant positive correlations are analyzed in the eastern Pacific and southern Caribbean SLP field (Fig. 9a). The influence of the eastern dipole of the Southern Oscillation is reduced over the Caribbean compared to boreal winter, while most other Atlantic SLP clusters correlate negatively with the SOI (significantly off Northwest Africa). As in the opposite season, most of the Indian Ocean SLP field is significantly negatively correlated with the SOI (ref. Walker and Bliss, 1932).

Wind speed and cloudiness cluster correlation fields fail to achieve 95% field significance in boreal summer (Table 2). Nevertheless, some correlations appear noteworthy in the context of all boreal summer fields. The northeast trades of the eastern Pacific (Fig. 3b) are weakened during the positive SO phase in July/August (Fig. 9b), whereas the southerly flow between the equator and 10° N is significantly enhanced (Fig. 9b). Complementing this result, Rasmusson and Carpenter (1982), Pazan and Meyers (1982), and Pan and Oort (1983) adduce evidence of weakened cross-equatorial flow into the east Pacific trough for the opposite negative SO phase.

Large portions of the South Atlantic trades (Fig. 3b) correlate positively with the SOI (Fig. 9b), although not at the 95% significance level. Pan and Oort (1983) analyzed marginally stronger trades for a positive SOI over the Atlantic on an annual basis. In connection with SLP clusters to the south of the near-equatorial trough axis that tend to correlate higher positively or less negatively with the SOI than the respective clusters to the north (Fig. 9a and 3a), significantly weakened trade winds immediately to the north of the trough (Fig. 9b) entail a tendency for a more northerly position of the Atlantic and eastern Pacific near-equatorial baric trough axis (Fig. 3a) for a positive SOI.

Most of the Indian Ocean wind field (Fig. 9b), including the southwest monsoon flow, correlates weakly with the SOI. Weak positive correlations with the SOI in the wind field over the Bay of Bengal (Cadet, 1985) are not regarded as significantly different from the present findings. Significant negative correlations are analyzed around Indonesia (Fig. 9b), translating into weakened cross-equatorial flow during the positive SO phase.

Increased cloudiness for a positive SOI over the northeastern Atlantic (positive correlations in Fig. 9c) supports the anomalously far northward position of the Atlantic near-equatorial trough inferred above from pressure (Fig. 9a) and wind (Fig. 9b) correlation patterns. Note that in contrast to boreal summer (Fig. 9) an anomalously far southerly location of the Atlantic trough during the positive SO phase was inferred for boreal winter (Fig. 8). Over large parts of the Indian Ocean, negatively correlated SLP (Fig. 9a) and positively correlated cloudiness (Fig. 9c), in particular over the Arabian Sea, suggest a concurrently enhanced monsoon in the positive SO phase. Increased monsoonal rainfall over the Indian subcontinent during the positive SO phase has been substantiated (Pant and Parthasarathy, 1981; Cadet, 1985; Wu and Hastenrath, 1986). However, strengthened monsoonal flow towards India cannot be corroborated from our results (weak correlations in Table 2). In a similar vein, Wu and Hastenrath (1986) analyzed only weak positive correlations between Arabian Sea surface wind speed and Indian summer rainfall for July and August.

The eastern Pacific SST field exhibits negative correlations with the SOI during July/August (Fig. 9d), as in January/February (Fig. 8d). The Atlantic sea surface appears devoid of any SO signal in boreal summer (Fig. 9d). The western and central Indian Ocean SST field correlates mostly negatively with the SOI, significantly

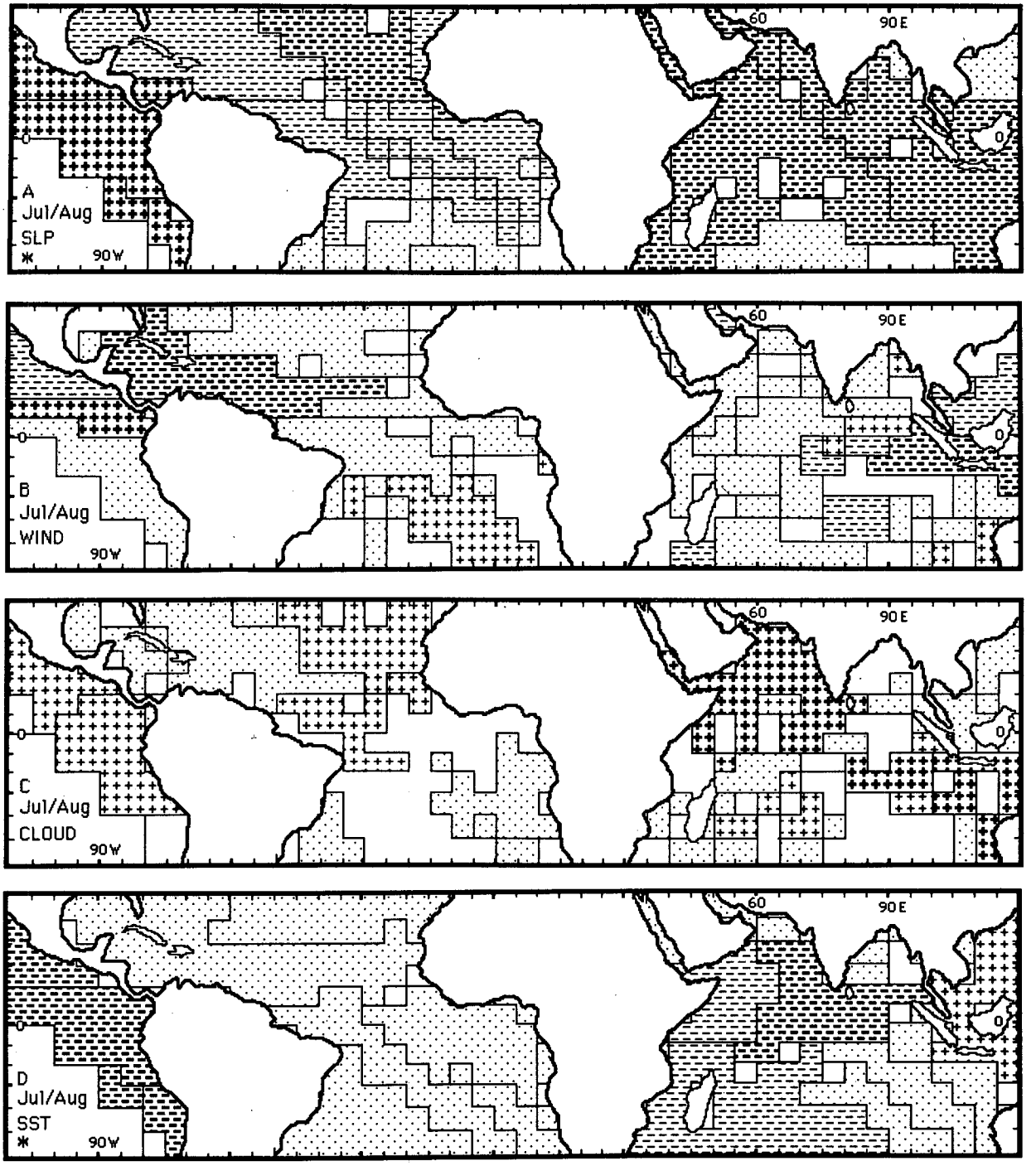

FIG. 9. As in Fig. 8, except for July/August correlation maps.

to the South of India (Fig. 9d), whereas in parts of the Bay of Bengal and in the eastern Indian Ocean anomalously high SST is associated with the positive SO phase (Fig. 9d). Simultaneously, the surface wind speed in the greater Indonesian region appears reduced, as inferred from significant negative correlations in Fig. 9b. Such an inverse relationship between SST and surface wind speed has been discussed earlier with reference to the general circulation setting about Indonesia (Nicholls, 1984; Hackert and Hastenrath, 1986).

In sum, the following general circulation behavior of the Southern Oscillation can be construed for the positive phase of this global pressure seesaw. The near-equatorial trough of the Atlantic appears located

anomalously far south in boreal winter, as is borne out by SLP (Fig. 8a), and wind speed cluster fields (Fig. 8b). By contrast, during boreal summer the Atlantic trough tends to be shifted to the north, as is inferred again from internally consistent evidence of SLP, wind, and cloudiness fields (Fig. 9a, b, c). The eastern Pacific trough appears to act in unison with the Atlantic trough in boreal summer (Fig. 9a, b). In both seasons, trade winds over the eastern Pacific are slack (Fig. 8b and 9b), while Atlantic trades are mostly strengthened over the respective winter hemisphere, in particular in January/February (Fig. 8b). For neither season is there conclusive evidence of sympathetic interannual variations in the latitude positions of the near-equatorial trough in the lower atmosphere and the zone of maximum ocean surface temperature.

Over the Indian Ocean, during both boreal winter and summer, SLP is lowered (Fig. 8a and 9a), while cloudiness is increased in the greater Indonesian area (Fig. 8c and 9c). In boreal winter, this is accompanied by a strengthening of the northeast monsoon flow (Fig. 8b). The implied enhanced convergence appears consistent with increased cloudiness (Fig. 8c) near the western dipole of the SO. In boreal summer, lowered SLP (Fig. 9a) and increased cloudiness (Fig. 9c), in particular over the Arabian Sea, suggest an enhanced southwest monsoon, although this is not substantiated by the patterns of wind correlation (Fig. 9b).

7. Conclusions

Cluster analysis is introduced as a useful tool for the examination of large-scale interannual climate variations. Its basic purpose here is to discover and delineate natural scales and regions of climate variability. This task is accomplished in a quasi-objective way, rendering the method reproducible and the clusters testable for statistical significance. According to a hierarchical organizing principle, intermediate clusters were selected in order to capture the large-scale spatial degrees of freedom of the field, averaging around 20° by 20° latitude-longitude. Monte Carlo simulations were used in order to ascertain the statistical significance of these clusters. About 75% to more than 90% of the original fields are represented by such tested clusters.

Fields of sea level pressure (SLP) and sea surface temperature (SST) show higher clustering similarities than those of surface wind speed and cloudiness. In the Atlantic, and in part in the eastern Pacific domain, the separation of all analyzed fields into zonally oriented clusters stands out, associated with trade wind systems to the north and south of the near-equatorial trough axis. By contrast, the Indian Ocean features strong meridional interhemispheric connections, in particular during the northern summer monsoon, emphasizing the oceanwide character of the monsoon system.

Characteristics of the Southern Oscillation are examined, as they reveal themselves in cluster fields of SLP, wind speed, cloudiness, and SST, in the tropical Atlantic, eastern Pacific, and Indian Oceans, correlated with an index of the Southern Oscillation (Parker, 1983). The concentration of all fields into a small number of large-scale clusters results in a high proportion of statistically significant relationships with the SO. This result was substantiated by Monte Carlo simulations that ascertained the field significance of all but two element–season correlation fields. In addition, the notion was corroborated that the clusters used here represent the large-scale degrees of freedom of the examined fields.

Most of the SLP correlation patterns with the SOI confirm previously known features of this global pressure seesaw. Similarly, a widespread anomalously cold sea surface during the positive SO phase has been described before. As a new result, the near-equatorial trough appears shifted northward during the positive SO phase in boreal summer over the Atlantic and eastern Pacific, and shifted southward in boreal winter over the Atlantic alone, as borne out by SLP, wind, and cloudiness cluster fields. Thus, the latitude position of the near-equatorial trough is inferred to be dependent on the phase of the Southern Oscillation in a seasonally varying manner for the Atlantic Ocean. In addition, Atlantic trades appear strengthened during the positive SO phase in the respective winter hemisphere, while eastern Pacific trade winds are weakened.

Over the Indian Ocean, during the positive SO phase, SLP is lowered, while cloudiness is increased in the greater Indonesian region—a feature familiar from previous SO descriptions. In boreal winter, this is accompanied by an enhancement of the northeast monsoon flow and of the southeast trades, the inferred enhanced convergence being consistent with increased cloudiness near the western dipole of the SO. Over the western Indian Ocean, during boreal summer in the positive SO phase, lowered SLP and increased cloudiness, in particular over the Arabian Sea, suggest an enhanced southwest monsoon.

All three tropical domains, i.e. Atlantic, eastern Pacific, and Indian Ocean, participate coherently in the Southern Oscillation, as captured in cluster correlation fields. The Atlantic and eastern Pacific troughs behave highly synchronously with respect to the SO in July/August, despite differing actions of the respective oceanic trades. In the Indian Ocean, both northeast and southwest monsoon systems partake in the general circulation functioning of the Southern Oscillation. Hence, all major tropical circulation components over the Atlantic, eastern Pacific, and Indian Oceans interact with the Southern Oscillation, and serve as prime movers for the associated interannual climate variations.

Acknowledgments. The author wishes to thank Professor Stefan Hastenrath for making available the ship data used here, and for useful discussions prior to and

during the completion of this manuscript. Discussions with Patricio Aceituno, in particular about the Monte Carlo testing philosophy, are gratefully acknowledged. Two anonymous reviewers are thanked for their comments, encouraging the author to explain in more depth and detail the employed cluster analysis technique. This study was supported by NSF Grant ATM84-13575 and NOAA Grant NA86 AA-D-AC064.

REFERENCES

Anderberg, M. R., 1973: *Cluster Analysis for Applications.* Academic Press, 359 pp.

Barnett, T. P., and R. W. Preisendorfer, 1978: Multifield analog prediction of short-term climate fluctuations using a climate state vector. *J. Atmos. Sci.*, **35**, 1771–1787.

Berlage, H. P., 1966: The Southern Oscillation and World Weather. Koninklijk Nederlands Meteorologisch Instituut, Mededelingen en Verhandelingen No. 88, 152 pp.

Bjerknes, J., 1969: Atmospheric teleconnections from the equatorial Pacific. *Mon. Wea. Rev.*, **97**, 163–172.

BMDP, 1983: *BMDP Statistical Software.* University of California Press, 735 pp.

Cadet, D. L., 1985: The Southern Oscillation over the Indian Ocean. *J. Climatol.*, **5**, 189–212.

Chen, W. Y., 1982: Assessment of Southern Oscillation sea level pressure indices. *Mon. Wea. Rev.*, **110**, 800–807.

Egger, J., G. Meyers and P. B. Wright, 1981: Pressure, wind and cloudiness in the tropical Pacific related to the Southern Oscillation. *Mon. Wea. Rev.*, **109**, 1139–1149.

Gadgil, S., and R. N. Iyengar, 1980: Cluster analysis of rainfall stations of the Indian peninsula. *Quart. J. Roy. Meteor. Soc.*, **106**, 873–886.

Galliani, G., and F. Filippini, 1985: Climatic clusters in a small area. *J. Climatol.*, **5**, 487–501.

Hackert, E., and S. Hastenrath, 1986: Mechanisms of Java rainfall anomalies. *Mon. Wea. Rev.*, **114**, 745–757.

Hartigan, J. A., 1975: *Clustering Algorithms.* Wiley and Sons, 351 pp.

Hastenrath, S., 1985: *Climate and Circulation of the Tropics.* Reidel, 455 pp.

——, and P. J. Lamb, 1977: *Climatic Atlas of the Tropical Atlantic and Eastern Pacific Oceans.* University of Wisconsin Press, 112 pp.

——, and P. J. Lamb, 1979: *Climatic Atlas of the Indian Ocean. Part 1. Surface Climate and Atmospheric Circulation.* University of Wisconsin Press, 116 pp.

——, and M. C. Wu, 1982: Oscillations of upper-air circulation and anomalies in the surface climate of the tropics. *Arch. Meteor. Geophys. Bioklim.*, **B31**, 1–37.

Johnson, R. A., and D. W. Wichern, 1982: *Applied Multivariate Statistical Analysis.* Prentice-Hall, 594 pp.

Lawson, M. P., R. C. Balling, Jr. and A. J. Peters, 1981: Spatial analysis of secular temperature fluctuations. *J. Climatol.*, **1**, 325–332.

Livezey, R. E., and W. Y. Chen, 1983: Statistical field significance and its determination by Monte Carlo techniques. *Mon. Wea. Rev.*, **111**, 46–59.

Newell, R. E., R. Selkirk, and W. Ebisuzaki, 1982: The Southern Oscillation: sea surface temperature and wind relationships in a 100-year data set. *J. Climatol.*, **2**, 357–373.

Nicholls, N., 1984: The Southern Oscillation and Indonesian sea surface temperature. *Mon. Wea. Rev.*, **112**, 424–432.

Pan, Y. H., and A. H. Oort, 1983: Global climate variations connected with sea surface temperature anomalies in the eastern equatorial Pacific Ocean for the 1958–73 period. *Mon. Wea. Rev.*, **111**, 1244–1258.

Pant, G. B., and B. Parthasarathy, 1981: Some aspects of an association between the Southern Oscillation and Indian summer monsoon. *Arch. Meteor. Geophys. Bioklim.*, **B29**, 245–252.

Parker, D. E., 1983: Documentation of a Southern Oscillation index. *Meteor. Mag.*, **112**, 184–188.

Pazan, S. E., and G. Meyers, 1982: Interannual fluctuations of the tropical Pacific wind field and the Southern Oscillation. *Mon. Wea. Rev.*, **110**, 587–600.

Pickard, G. L., and W. J. Emery, 1982: *Descriptive Physical Oceanography.* Pergamon, 249 pp.

Quenouille, M. H., 1952: *Associated Measurements.* Butterworths, 241 pp.

Rasmusson, E. G., and T. H. Carpenter, 1982: Variations in tropical sea surface temperature and surface wind fields associated with the Southern Oscillation/El Niño. *Mon. Wea. Rev.*, **110**, 354–384.

Reiter, E. R., 1979: Trade-wind variability, Southern Oscillation, and quasi-biennial oscillation. *Arch. Meteor. Geophys. Bioklim.*, **A28**, 113–126.

Storch, H. V., and G. Hannoschöck, 1985: Statistical aspects of estimated principal vectors (EOFs) based on small sample sizes. *J. Climate Appl. Meteor.*, **24**, 716–724.

Troup, A. J., 1965: The Southern Oscillation. *Quart. J. Roy. Meteor. Soc.*, **91**, 490–506.

Walker, G. T., and E. W. Bliss, 1932: World weather V. *Mem. Roy. Meteor. Soc.*, **4**, 53–84.

Wright, P. B., 1985: The Southern Oscillation: An ocean-atmosphere feedback system? *Bull. Amer. Meteor. Soc.*, **66**, 398–412.

Wu, M. C., and S. Hastenrath, 1986: On the interannual variability of the Indian monsoon and the Southern Oscillation. *Theor. Appl. Climatol.*, **36**, 239–261.